ADVANCED OPTICAL MATERIALS

Supporting Information

Underwater Self-Powered All-Optical Wireless Ultrasonic Sensing, Positioning and Communication with Ultrafast Response Time and Ultrahigh Sensitivity

Zhen Tian, Li Su,* Haoyu Wang, Hongqiang Wang, and Yunlong Zi*

Supporting Information

Underwater Self-Powered All-Optical Wireless Ultrasonic Sensing, Positioning and Communication with Ultrafast Response Time and Ultrahigh Sensitivity

Zhen Tian, Li Su,* Haoyu Wang, Hongqiang Wang, and Yunlong Zi*

Table S1. Comparison of SNR value for the ultrasounic sensor with differnent working principle.

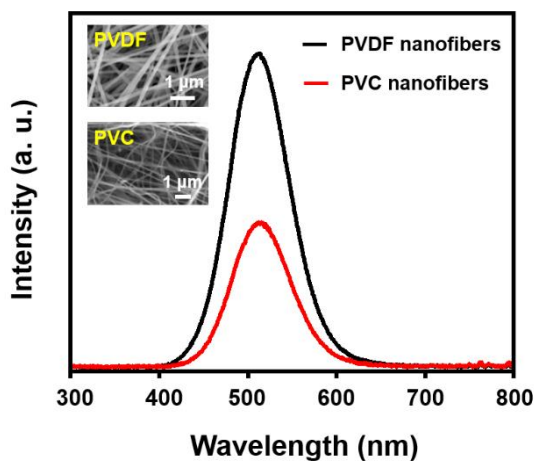| Specifications	Working principle	Ultrasonic frequency	SNR
Zhang *et al*.[1]	Capacitive	400 kHz	3 dB
Zhou *et al*.[2]	Piezoelectric	100-180 kHz	>12 dB
Chen *et al*.[3]	Piezoelectric	2.24 MHz	6 dB
Chen *et al*.[4]	Triboelectric	1 MHz	20.54 dB
Lee *et al*.[5]	Trboelectric	20 kHz	10.45 dB
Jiang *et al*.[6]	Fiber-optic	40 kHz	14.45 dB
Wei *et al*.[7]	Fiber-optic	10 MHz	20 dB
This Work	TIEL	40 kHz	26.02 dB

Figure S1. Luminescence intensity of two controlled SAWSs based on PVDF and piezoelectricity-free PVC nanofibers, respectively. Despite being less negative and piezoelectricity-free, PVC maintained a high level of luminescence intensity, which suggested that this characteristic of the SAWS-based on electrospun PVDF nanofibers was principally attributed to triboelectric rather than piezoelectric effect. Inset: SEM images of PVDF and PVC nanofibers.
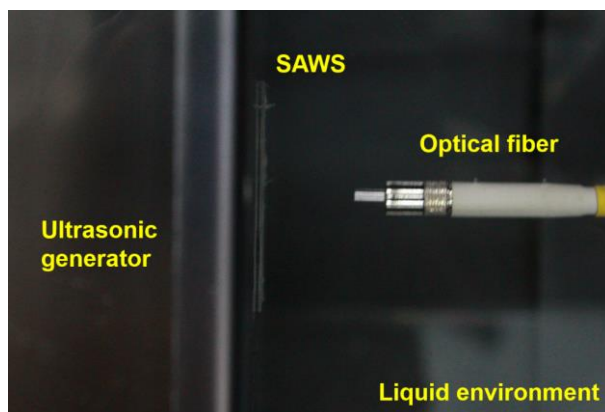
Figure S2. Construction of the test platform to investigate the major influential factors for the TIEL intensity of the SAWS.
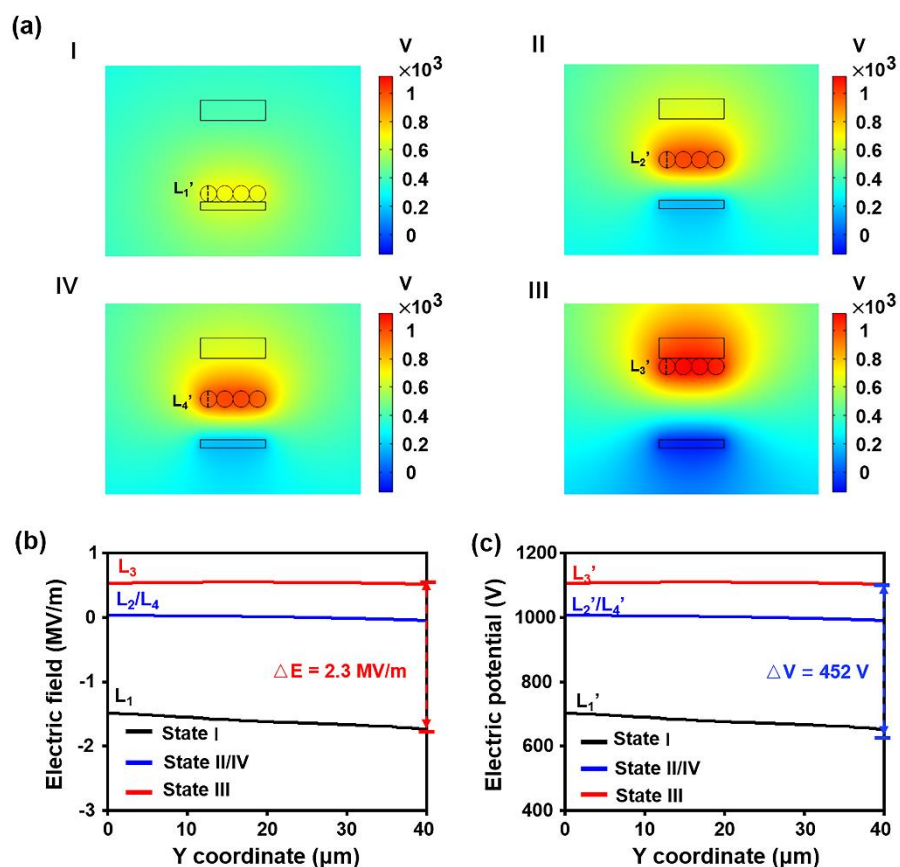
Figure S3. a) Numerical calculation of the potential distribution of the SAWS within a full contact-separation cycle in the four states, using COMSOL software. b) One-dimensional (1D) electric field and c) potential distribution of ZnS:Cu phosphors along the dashed lines in Figure 2d and Figure S3a.
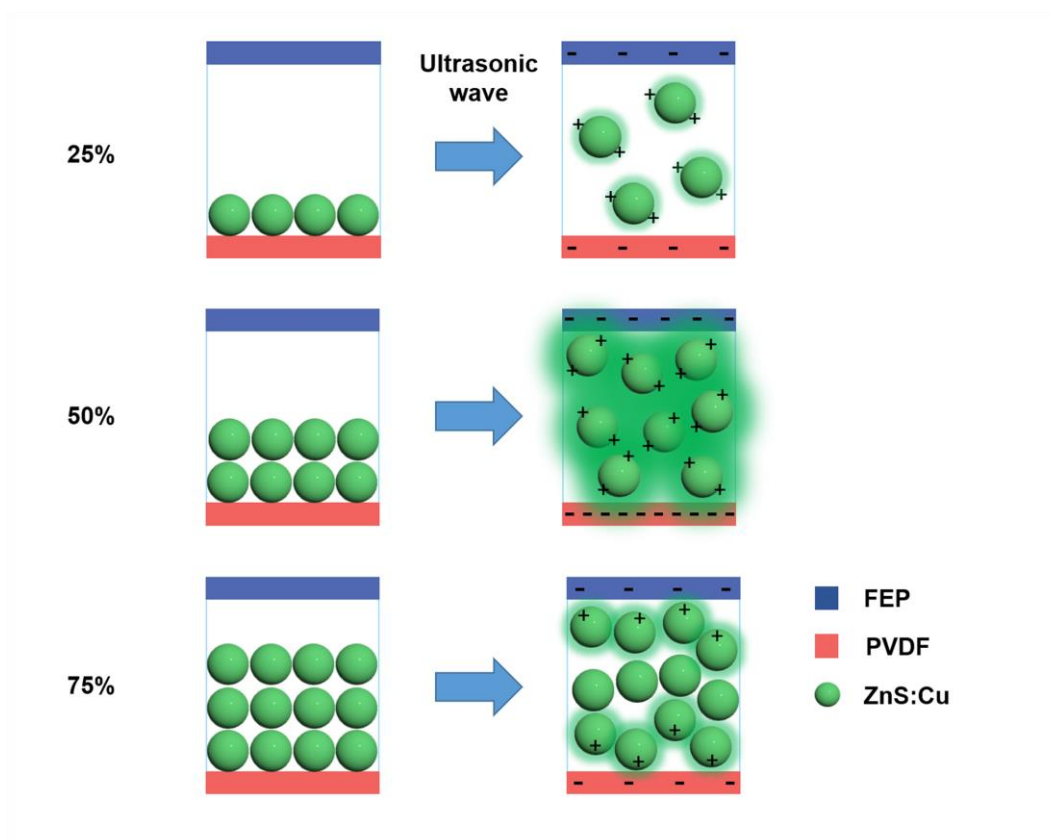
Figure S4. Illustration of the TIEL process of the SAWS when the cavity was filled with different amounts of ZnS:Cu particles.
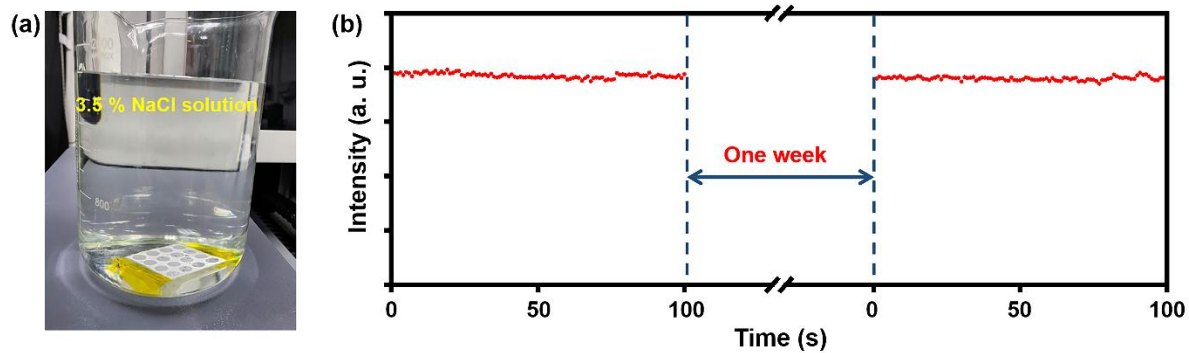
Figure S5. Comparison of the luminescent performance of SAWS before and after being immersed in 3.5 % NaCl solution for one week. a) Photograph of the immersed SAWS. b) The measured TIEL intensity.
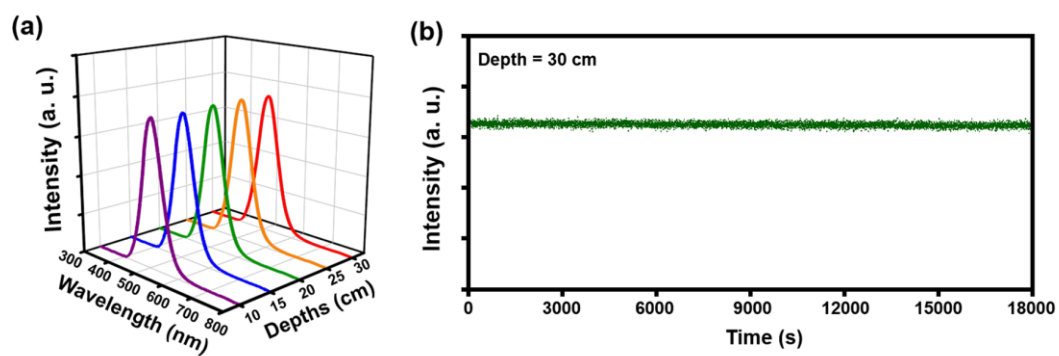
Figure S6. The effect of underwater working depth of SAWS. a) TIEL intensity of SAWS at different depths from 10 to 30 cm underwater. b) Stability of SAWS at a depth of 30 cm underwater.
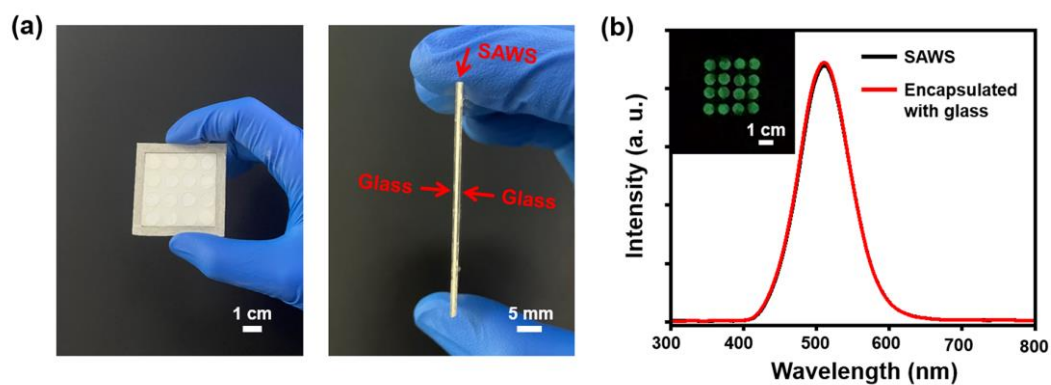
Figure S7. Comparison of the luminescent performance of SAWS before and after being encapsulated with glass. a) Photographs of the encapsulated SAWS. b) The measured TIEL intensity. Inset: luminescent photograph of the encapsulated SAWS with underwater ultrasonic wave excitation.
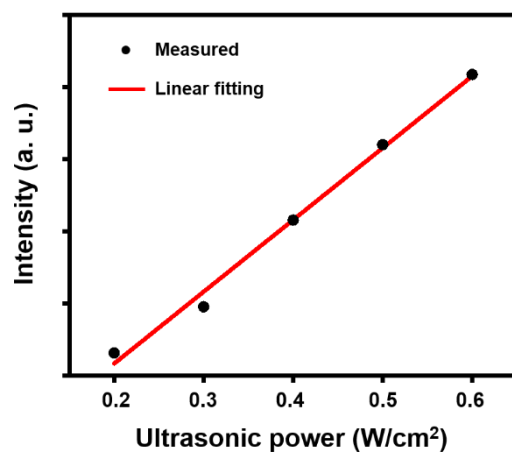
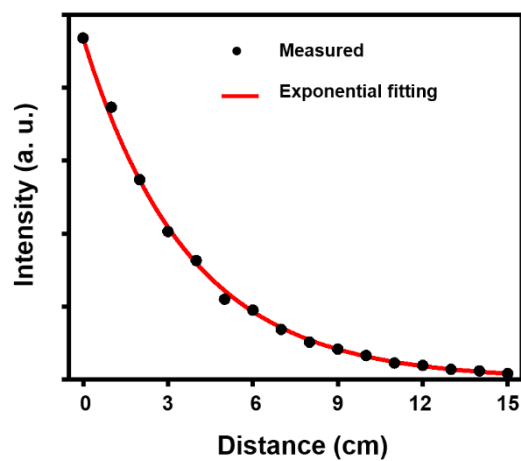**Figure S8.** Linear fitting results of measured intensity values under different ultrasonic powers.

Figure S9. Exponential fitting results of measured intensity values at a varying distance (0 to 15 cm) from the ultrasonic source. The value of α in equation (2) is 0.269.

Note S1. Description of the EL/PL/ML spectrum

ZnS:Cu and polydimethylsiloxane (PDMS) were mixed at a ratio of 1:1 to obtain a ZnS:Cu/PDMS film, and two transparent electrodes were combined with upper and lower surfaces. The EL spectrum was obtained with the alternating current diver of 50 Hz, whose wavelength peak was centered at 516 nm, as shown in Figure 3c. The PL spectrum of ZnS:Cu/PDMS was obtained by a fluorescence spectrometer (FLS920, Edinburgh Instruments, Britain) under the excitation of 365 nm UV, whose wavelength peak position was centered at 518 nm. The ML spectrum of ZnS:Cu powders could be derived under a contact pressure of 5 MPa, whose wavelength peak position was 522 nm. Notably, the characteristics of ML, EL, and PL spectrum are almost similar. Regarding the characteristics of TIEL under the excitation of an ultrasonic wave (40 kHz, 0.6 W cm^{-2}), however, the wavelength peak of the SAWS had to be centered at 510 nm, as shown in Figure 2b**.** The difference between TIEL and other emission spectra was attributed to the high frequency (produced by the ultrasonic waves) of the alternating electric field applied to ZnS:Cu phosphors. When the frequency of the alternating electric field increased, electrons transferred from the shallow electronic trap to the e rather than t$_2$ level of Cu^{2+}, resulting in the shift of the spectrum.

Note S2. The explanation of the filling ratio

Since the movement of ZnS particles is uniform and random, the electric field is mainly determined by the tribo-charge density during triboelectrification.[8,9]

The filling ratio was defined by the volume ratio of zinc sulfide to the cavity in this study. As illustrated in Figure S4, when the filling ratio increases, the amount of ZnS involved in triboelectrification will increase, thus resulting in the raised tribo-charge density. However, when the filling ratio is too high, the collision contact area between ZnS particles and FEP/PVDF will decrease due to the reduced vibration ability, thus causing the weakened TIEL intensity. Besides, the light-shielding caused by the high filling ratio is also a reason for its decreased intensity. Based on the experimental results, the TIEL intensity reaches the maximum value when the filling ratio was 50%.

Note S3. The estimation of the working depth range of SAWS underwater

We placed SAWS at different depths in the water tank (from 10 cm to 30 cm), where the TIEL intensity and stability were basically unchanged (Figure S6). As shown in Figure 3f, when the filling ratio increases by 16.7% (from 50% to 66.7%), the TIEL intensity of SAWS reduces by only about 20%. Thus, it is reasonable to suppose that the SAWS can work almost unaffectedly when the top FEP film is deformed to 5% of the cavity height. Then, the underwater working depth (H_w) of SAWS can be calculated through the following formula:

$$P_0 + \rho g H_w = P_a = \frac{1}{1-\frac{5\%}{F}} P_0 \tag{1}$$

where P_0 and P_a refer to standard air pressure and air pressure in the cavity, ρ is the density of seawater, g is the gravitational acceleration. F represents the filling ratio, which is 50%. Through calculation, H_w=1.1 m. That means our device can work properly in an underwater depth range of 1.1 m.

Moreover, according to the previous reports,[4] on the basis of the thin plate theory, the average displacement (u_{avg}) of the packaging material can be defined as:

$$u_{avg} = \frac{P a^4 (1-v^2)}{16 E t^3} \tag{2}$$

where P is the total pressure (induced by water and air) onto the packaging material, a is its radius. E and v refer to Young's modulus and Passion ratio of the packaging material, and t is thickness. For applications in the deep sea, since the SAWS is an ultra-thin (400 μm) film structure, which is very convenient for packaging, integration, and fixation, its working depth in practical applications can greatly improve through packaging with transparent rigid materials . Figure S7 shows the photographs and luminescent performance of SAWS packaged with glass (E =72000 MPa, v=0.2, and t=600 μm). The TIEL intensity and stability are little affected compared with the SAWS without a package. After calculation by Equation (2), the device can be used at underwater depths of larger than 300 m with an average deformation of

about 1 μm only, which means that our SAWS can be used at different depths based on actual requirements through simple packaging.

References

[1] R. Zhang, W. D. Zhang, C. D. He, J. L. Song, L. F. Mu, J. Cui, *Sensor Rev.* **2015**, *36*, 77.

[2] Z. Zhou, S. Yoshida, S. Tanaka, *Sensor Actuat. A-Phys.* **2017**, *266*, 352.

[3] Y. Chen, X. L. Bao, C.-M. Wong, J. Cheng, H. D. Wu, H. Z. Song, X. R. Jia, S. H. Wu, *Ceram. Int.* **2018**, *44*, 22725.

[4] C. Chen, Z. Wen, J. H. Shi, X. H. Jian, P. Y. Li, J. T. W. Yeow, X. H. Sun, *Nat. Commun.* **2020**, *11*, 4143.

[5] K. H. Lee, Y.-Z. Zhang, Q. Jiang, H. Kim, A. A. Alkenawi, H. N. Alshareef, *ACS Nano* **2020**, *14*, 3199.

[6] J. F. Jiang, T. H. Zhang, S. Wang, K. Liu, C. Li, Z. X. Zhao, T. G. Liu, *J. Lightwave Technol.* **2017**, *35*, 5079.

[7] H. M. Wei, S. Krishnaswamy, *Opt. Lett.* **2017**, *42*, 2655.

[8] C. B. Han, T. Jiang, C. Zhang, X. H. Li, C. Y. Zhang, X. Cao, Z. L. Wang, *ACS Nano* **2015**, *9*, 12552.

[9] Y. Xi, J. Wang, Y. L. Zi, X. G. Li, C. B. Han, X. Cao, C. H. Guo, Z. L. Wang, *Nano Energy* **2017**, *38*, 101.

Movie S1.

Luminescent array (4 × 4) excited by underwater ultrasonic waves (40 kHz and 0.6 W/cm^2).

Movie S2.

Luminescent letter "D" excited by underwater ultrasonic waves (40 kHz and 0.6 W/cm^2).

Movie S3.

Wind-driven mode of SAWS (15 m/s).

Movie S4.

Luminescence intensity variation of SAWS under different ultrasonic power inputs (0.2 W/cm^2 ~ 0.6 W/cm^2).

Movie S5.

Ultrasonic source positioning by multichannel SAWSs with a customized data acquisition system.

Movie S6.

Real-time optical signal communication by SAWS.